Sophia Antipolis, Côte d'Azur, France, 29 Sept. – 1 Oct. 2004

NON-CONTACT TRANSIENT TEMPERATURE MAPPING OF ACTIVE ELECTRONIC DEVICES USING THE THERMOREFLECTANCE METHOD

Mihai G. BURZO, Pavel L. KOMAROV, and Peter E. RAAD[†]

Department of Mechanical Engineering
Nanoscale Electro-Thermal Sciences Laboratory
Southern Methodist University
Dallas, TX 75275-0337, U.S.A

ABSTRACT

This article presents a proof of concept for an experimental methodology capable of non-invasively scanning with submicron spatial resolution the transient surface temperature of pulsed devices. The ultimate goal is to use the temperature scan as input for an inverse computational solution to fully characterize the thermal behavior of complex three-dimensional devices. This work describes the features of the experimental setup, provides details of the calibration process used to map the changes in the measured surface reflectivity to absolute temperature values, and explains the data acquisition procedure used to measure the temperature at a given location. To illustrate the experimental approach, both quasi-steady and transient temperature measurement results are presented for typical CMOS devices.

1. INTRODUCTION

Knowledge of the thermal behavior of a microelectronic device is crucial for improving its performance and reliability. As a result, there is an increased demand for methods to determine the temperature of submicron level features. Temperature can be measured by a diverse array of methods. All methods infer temperature by sensing some change in a physical characteristic. However, in order to measure the active junctions of modern devices, which are frequently powered in a pulsed mode, a method needs to have superior spatial and temporal resolutions. The use of contact methods presents the added difficulties of having to access features of a submicron device with an external probe, or in the case of embedded features, fabricate a measuring probe into the device, and then having to isolate and exclude the influence of the measuring probe itself. Even then, since in the case of submicron devices the thermal capacitance of the junction is extremely small, contact methods cannot be used if accurate measurements are desired. Consequently, non-contact, optical methods are usually preferred.

Among the various optical methods, the thermoreflectance method possesses important advantages and is so far the only method that has been employed to make submicron temperature mappings [1-3]. The main advantage of the TTR method is that it is a non-contact and non-destructive optical approach for probing steady-state and transient surface temperature, providing accurate results for submicron features of microelectronic devices with good temporal resolution.

The most challenging aspect for thermoreflectance measurements is the small value of the thermoreflectance coefficient of the top layer material, C_{th}, which defines the rate of change in the surface reflectivity as a function of the change in surface temperature, i.e., $C_{th} = \frac{1}{R}\frac{\Delta R}{\Delta T}$. The C_{th} coefficient needs to be sufficiently high in order to obtain an appropriate signal-to-noise ratio in the measurements. Usually, it must be higher than 10^{-5} per Kelvin for thermoreflectance temperature measurements to be obtainable with good accuracy. The most important parameters that influence C_{th} are the material under test and the wavelength of the probing laser.

The aim of this article is to report on the development and characterization of an experimental methodology capable of non-invasively scanning with submicron spatial resolution the transient surface temperature of pulsed devices. The system's capabilities are demonstrated by scanning the active area of typical CMOS devices of differing gate widths and lengths. Both steady-state and transient temperature measurement results are presented. The temporal and spatial limitations of the methodology are also discussed.

[†] Corresponding Author. Email: praad@smu.edu; Tel : 214-768-3866; Fax: 214-768-4998

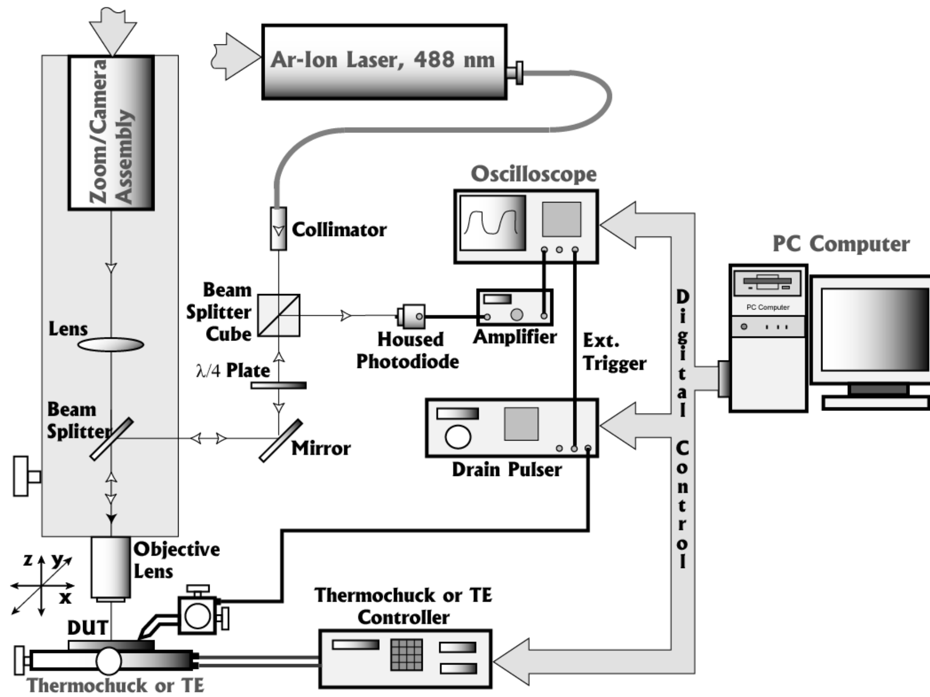

Fig. 1 Schematic of the experimental setup

2. EXPERIMENTAL METHODOLOGY

This section describes the features of the experimental setup, provides details of the calibration process used to map the changes in the measured surface reflectivity to absolute temperature values, and explains the data acquisition procedure used to measure the temperature at a given location with minimum random noise.

2.1. Experimental setup

The newly built temperature mapping experimental system at the SMU NETS Laboratory is depicted schematically in Fig. 1. The probing light source is an Ar-Ion CW laser with a linearly polarized, single-mode irradiation beam at a wavelength of 488 nm. The beam is delivered to the microscope assembly via a polarization preserving, fiber optic cable with TEM_{00} mode. Delivering the probing laser energy by a fiber makes it possible to easily incorporate lasers of different wavelengths to maximize the C_{th}. This is an important issue since, as shown by Tessier et al. [4], the thermoreflectance coefficient of a specific material is extremely sensitive to the wavelength of the laser and varies strongly between materials. The data presented for Al, Au, Cu, and Ni by Rosei and Lynch [5], Hanus et al. [6], and Scouler [7] confirm the fact that the C_{th} coefficient is wavelength dependent.

A beamsplitter cube and l/4 retardation plate are used to minimize losses through the probing optical path. The microscope objective lens focuses the laser light on the device under test (DUT), normal to its surface. The probing beam reflects from the heated surface back along the optical path to the sensitive area of a photodiode. The intensity of the reflected light depends on the reflectivity (temperature) of the sample's surface. The photodiode signal, containing the change in surface reflectivity caused by the temperature variations of the DUT, is acquired with an 8-bit resolution via a digital oscilloscope at a rate of up to 2 Giga-samples per second. This sampling rate allows the measurement of a transient temperature field of a DUT activated in the pulse mode with frequencies of up to 50 MHz, which provides 40 data points to describe a full heating and cooling cycle.

The integrated microscope and CCD camera system is mounted on a Cascade Microtech Alessi precision probing station, making it possible to view the DUT and to position the laser beams on its surface with a resolution of 0.5 μm. The microscope has a motorized, 40X continuous zoom capability. Five microscope objective lenses (5X, 10X, 20X, 50X and 100X) are available, providing a maximum magnification of 4000X. The smallest probing spot is that can be achieved with the current system is 0.7 μm. The device under test is placed on a Temptronic, 8-inch, liquid-stabilized thermal chuck, capable of maintaining the bottom of the device substrate at an isothermal condition, in the range of 0 - 200°C.

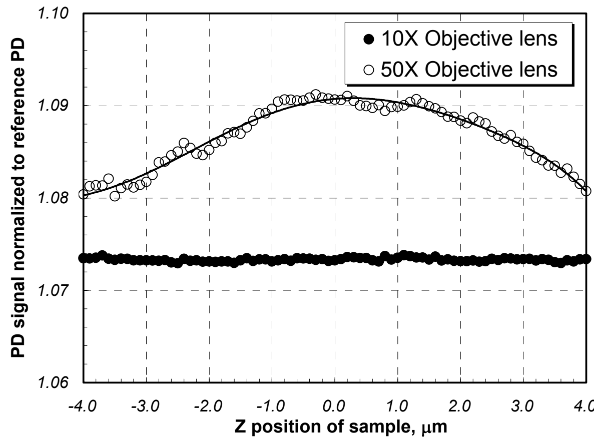

Fig. 2 Out-of-focus and interference parasitic effects for the 10X and 50X objective lenses.

2.2. Calibration

Initially, the thermal chuck was used to generate a temperature-reflectivity calibration curve (from which one can determine the thermoreflectance coefficient, C_{th}). However, uncontrolled movements of the chuck surface result in significant planarity distortion, which in turn make it impossible to distinguish the desired thermal reflectance. To avoid the parasitic effects associated with the thermal expansion of the relatively massive thermochuck, a smaller (30×30×5 mm) thermoelectric (TE) device was used to calibrate the measurements. The calibration approach consists of determining the dependence between the change in the reflectance and the change in the surface temperature. The change in reflectance was measured by a differential scheme involving two identical PDs in order to minimize the influence of fluctuations in the energy output of the probing laser. In this approach, the laser light is divided into two beams, one collected on the reference PD and the other collected on the second PD after being reflected from the sample surface. The sample temperature is measured with a 0.1 mm K-type thermocouple. The calibration must be performed for each of the materials on the surface of each device where a mapping of the temperature is carried out.

The reflectance coefficient is normally very small (on the order of 10^{-4} for gold covered with a silicon oxide passivation layer), and therefore parasitic effects must be minimized in its measurements. Notably, Dilhaire et al. [9] have pointed out that the thermoreflectance calibration procedure can be hindered by the movement of the device under test as a result of the thermal expansion of the heater used to heat and position the device. This movement generates both interferometric and out-of-focus parasitic effects in the photodetector signal. The out-of-focus effect is more significant if a high numerical aperture (NA) objective lens is used in the measurements. Given the potential negative implications of the aforementioned parasitic effects, tests were designed and carried out to help assess the magnitude of these effects in the present system.

First, a reflective sample was held on a Z-axis translation stage (i.e., along the optical axis of the objective lens) whose resolution is 0.1 µm. While moving the sample up and down from the plane of focus of the objective lens, the resulting signal was measured by a differential scheme that uses two identical PDs. The results for two objective lenses (10X and 50X) with different numerical apertures (NA = 0.28 and 0.42, respectively) are presented in Fig. 2.

As expected, the measurements with the high NA objective lens are more sensitive to the out-of-focus effect than those with the low NA lens. However, unlike in the case of the system reported on by Dilhaire et al. [9], no interferometric effect was detected in the PD signal for either objective lens. Specifically, in order to have an interferometric effect, a regular sinusoidal pattern in the PD signal must be present. For a Fabry-Perot interferometer, the expected period of the pattern should equal to $\lambda/2$, which in the SMU system is 244 nm. Even with the coarse resolution of the available translation stage (100 nm), which is comparable to the $\lambda/2$ period, the PD signal should exhibit a regular zigzag pattern when the interferometric effect is present in the system. The absence of such a pattern indicates that the interferometric effect is negligible or non existent.

To further confirm the absence of the parasitic Fabry-Perot interferometric effect in the SMU system, a second, simple but conclusive test was performed. The idea for the test originates from the fact that any interferometer must have at least two arms whose lights interfere on the sensitive area of a photodetector. As mentioned by Dilhaire et al. [9], for the thermoreflectance system one arm includes the sample surface while the other arm includes the input and output planes of the objective lens. This implies that if one arm were to be deactivated, the PD would detect the light from the other arm. Therefore, the test consists of blocking the reflected light from the sample and measuring the output PD signal that should be produced from the second arm, i.e., from the two planes of the objective lens. Observing that the output PD signal was nearly zero for either objective lens leads to the conclusion that there is no second arm interference present in the system used in this investigation.

Combining the results of this investigation with that of Dilhaire et al. [9] yields important guiding information, namely that the presence of parasitic interferometry effects should be tested for each new thermoreflectance system. If such effects are found to be present, they can be mitigated by minimizing back reflection and increasing the distance from the objective lens to the PD.

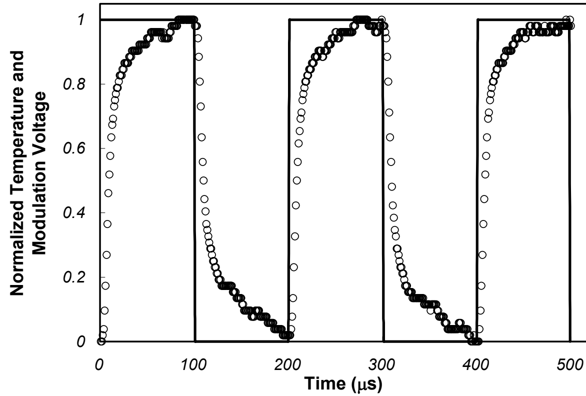

Fig. 3 Transient normalized temperature and modulation signal (at hottest point on a CMOS device)

2.3. Temperature data acquisition

Extracting the temperature value at a given point on the surface of an active device in the framework of the thermoreflectance method requires the measurement of the surface reflectivity at that point. This can be achieved by capturing on the photodetector the level of laser energy reflected back from the sample and comparing it to the calibrated data. However, given the small value of the coefficient of reflectivity, such an approach would have a very weak signal to noise ratio. To overcome this limitation, the activation voltage of the device is modulated, resulting in a modulated photodetector signal that can more easily yield the useful signal from the raw photodetector signal. The outcome of each data collection after a pulsed activation is a transient waveform, an example of which is shown in Fig. 3, superimposed on the modulated activation voltage. After averaging over 256 waveforms, each containing 500 data samples, the transient reflectivity signature at a physical location is obtained with good accuracy (in the range of 1 to 2%). Once the reflectivity is measured, the corresponding absolute temperature value can be calculated by scaling with the thermoreflectance coefficient.

The temperature field over a region of interest can be mapped by repeating the above procedure at multiple physical locations. The SMU system is designed to acquire the temperature at a point, which can be positioned with a resolution of 0.5 μm (in the x and y directions), and then automatically repeat the process over a grid covering the physical region of interest. This scanning process yields a transient temperature field over the desired surface area.

While the extent of the region of interest and the number of measurement points in it can be specified, acquisition time is a limiting factor. Presently, the system can measure the transient temperature at approximately 200 locations in an hour. At least two to three orders of magnitude speedup in the measurements is possible with faster electronics and the use of photodetector arrays.

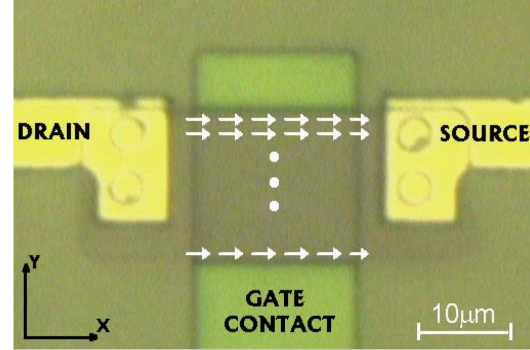

Fig. 4 Direction and placement of temperature scanning over the channel of a CMOS device

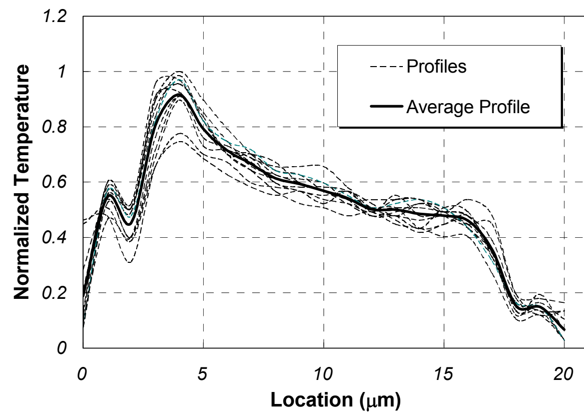

Fig. 5 Profiles of normalized temperature maxima along the channel (from Drain to Source) of the activated 18 × 15 μm device shown in Fig. 4 at different locations over the channel width

3. RESULTS AND DISCUSSION

To demonstrate the scanning methodology, experiments were conducted on typical CMOS devices. Figure 4 shows the channel region of a device with the measurement points depicted along rows crossing from the drain to the source. For the case described in conjunction with Fig. 3, the reflectivity reaches a maximum every 200 μs starting at around 100 μs. The amplitude of the waveform can be easily extracted and represents the rise in the reflectivity of the device at the measurement location. The reflectivity rise profile is recorded along the length of the channel (from drain to source) for 12 different paths across the channel width. Then, the profiles are normalized with respect to the highest reflectivity change recorded in the channel region. In addition, the 12 profiles are averaged to yield a single representative reflectivity profile along the channel. Once

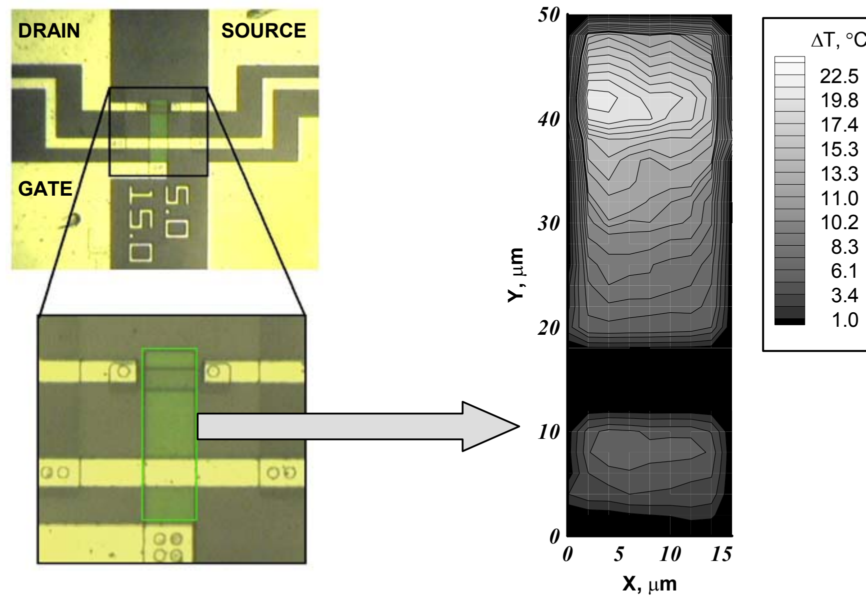

Fig. 6 Scan Area and corresponding temperature contours on an activated CMOS device at the time of peak temperature (channel dimensions are 15 × 5 μm)

normalized, the reflectivity rise and temperature rise profiles become identical. The 12 temperature rise profiles and their representative average are plotted in Fig. 5. As can be expected, the temperature distribution along the channel exhibits asymmetrical behavior with the peak temperature shifting toward the drain.

The channel region of a CMOS device with a smaller channel was scanned to demonstrate the method's capability of capturing the transient behavior of absolute surface temperature field. In each scan and at each measurement location, 256 waveforms of the photodetector signal were again averaged in order to reduce the random noise inherent in the system. Since the overall sampling capability of the system is more than 50 MHz (20 ns) and the timescale of the heat transfer (conduction) in microelectronic devices is usually in the microseconds (and up to milliseconds), the system has sufficient time resolution to capture the fastest possible heating/cooling processes. This fast temporal capability of the system is demonstrated by the temperature waveform previously shown in Fig. 3 superimposed on the activation pulsed signal. The full heating and cooling cycle in this case takes around 0.2 ms. Because of the modulation frequency and the 50% duty cycle, this device does not reach a quasi-steady temperature state.

The electric current used to activate the smaller device was pulse-modulated at 5 KHz and 50% duty cycle. The two-dimensional temperature contours for the 5 μm wide by 15 μm long junction device are shown on the right hand side of Fig. 6 at the time where the device experiences the highest temperature rise. The extent of the scanned area of the device is shown on the left hand side of the same figure. To produce the absolute temperature rise values in Fig. 6, the measured reflectivity field was scaled with the thermal reflectance coefficient. The latter was measured as described in section 2.2, but with a 10X objective lens in order to eliminate the parasitic effects associated with the previously discussed out-of-focus drawback.

The temperature rise ranges from nearly zero to about 25 °C in the channel, with the peak occurring closer to the drain of the device. The dark gap area near the bottom of the contour plot in Fig. 6 corresponds to the back contact metalization strip. Since this strip sits on top of the passivation layer, it is well insulated from the heat produced in the active channel and hence experiences an undetectable rise in temperature.

To further demonstrate the capability of the system to provide transient surface temperature behavior, snapshots of an animation of the temperature contours are shown in Fig. 7. The eight snapshots represent the surface temperature field at 15 μs increments during the heating phase and the beginning portion of the cooling phase of the full pulsed cycle.

This paper presented a proof of concept of an experimental methodology capable of mapping the transient surface temperature of an active device operated in pulsed mode. This work is a part of an integrated approach whose aim is to characterize the transient thermal behavior of fully-featured 3D structures. The overall approach uses the described experimental technique to non-invasively scan the surface temperature where possible and then solves an inverse numerical problem with an ultra-fast adaptive technique to

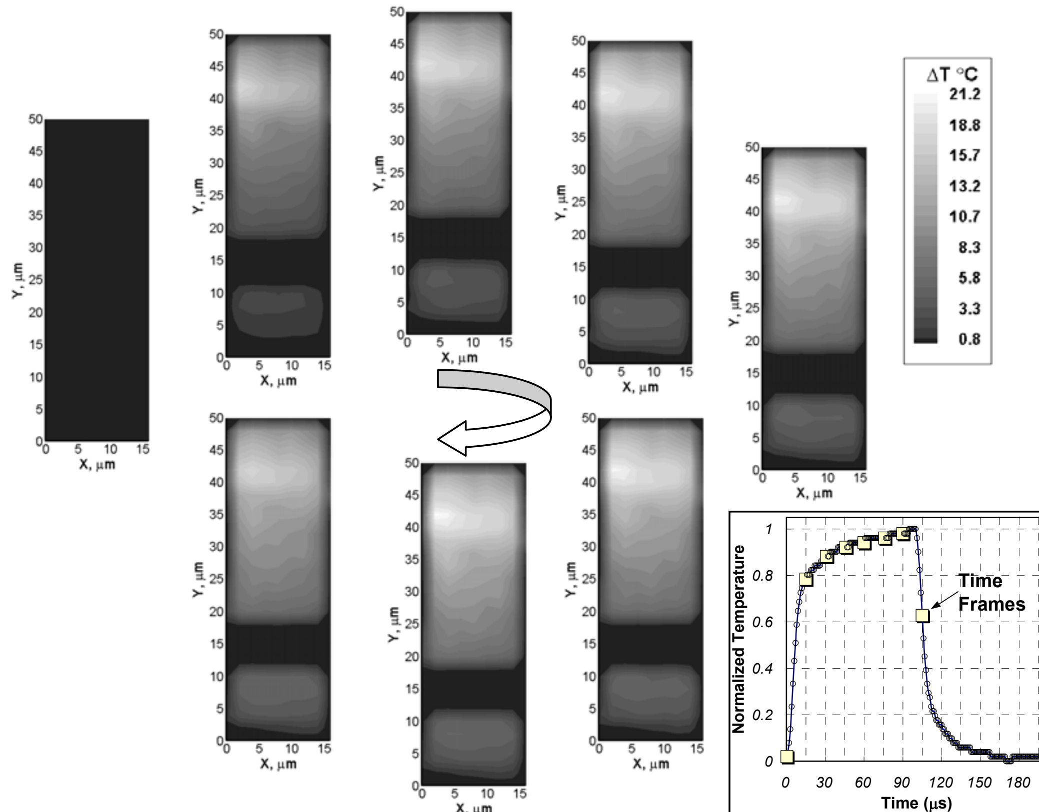

Fig. 7 Temperature contours for the activated device shown in Fig. 5 during the heating phase of a pulse cycle (15 µs between frames)

determine the temperature distribution over the entire 3D device, including important embedded features whose response is otherwise impossible to measure directly.

4. ACKNOWLEDGMENTS

The authors are grateful to Prof. Sanjay Banerjee and his research assistant Lisa Weltzer of University of Texas at Austin for providing the CMOS devices.

5. REFERENCES

[1] K.E. Goodson and Y.S. Ju, “Short-time-scale Thermal Mapping of Microdevices using a Scanning Thermoreflectance Technique,” *Trans. of the ASME*, pp. 306-313, May 1998.

[2] S. Grauby, S. Hole, and D. Fournier. “High Resolution Photothermal Imaging of High Frequency Using Visible Charge Couple Device Camera Associated with Multichannel Lock-in Scheme,” *Review of Scientific Instruments*, pp. 3603-3608, 1999.

[3] V. Quintard, S. Dilhaire, T. Phan, and W. Claeys, “Temperature Measurement of Metal Lines under Current Stress by High Resolution Laser Probing,” *IEEE Trans. on Instrumentation and Measurement*, pp. 69-74, Feb. 1999.

[4] G. Tessier, S. Hole, and D. Fournier, ”Quantitative Thermal Imaging by Synchronous Thermoreflectance with Optimized Illumination Wavelengths,” *Applied Physics Letters*, Vol. 78, pp. 2267-2269, 2001.

[5] R. Rosei, and D.W. Lynch, “Thermomodulation Spectra of Al, Au, and Cu,” *Phys. Rev. B*, Vol. 5, pp. 3883-3893, 1972.

[6] J. Hanus, J. Feinleb, and W.J. Scouler, “Low-energy Interband Transitions and Band Structures in Nickel,” *Physical Review Letters*, Vol. 19, pp.16-20, 1967.

[7] W.J. Scouler, “Temperature Modulated Reflectance of Gold from 2 to 10 eV,” *Phys Review Letters*, Vol. 18, pp. 445-448, 1967.

[8] G. Kaytaz, P. L. Komarov, and P. E. Raad, “A New Simulation Model of Electro-Thermal Degradation for MOSFET Devices Subjected to Hot Carrier Injection Stress,” *9th International IEEE Workshop on THERMal INvestigations of ICs and Systems (THERMINIC 2003)*, Aix-en-Provence, France, pp. 251-256, September 24-26, 2003.

[9] S. Dilhaire, S. Grauby, and W. Claeys, “Calibration procedure for temperature measurements by thermoreflectance under high magnification conditions,” *Applied Physics Letters*, Vol. 84, pp. 822-824, 2004.